CHAPTER VI
VS-1 ZEOLITE SYNTHESIZED DIRECTLY FROM SILATRANE

6.1 Abstract

VS-1 zeolite was successfully synthesized using silatrane as the precursor via sol-gel processing and microwave heating methods. Various factors, which influence the product properties, were investigated, viz. water content, reaction temperature, sodium hydroxide concentration, and amount of vanadium loading. XRD, SEM, UV-visible and ESR were applied to characterize synthesized VS-1. Lower water content and higher temperature promote incorporation of vanadium in the zeolite structure, and lower sodium hydroxide concentration gives more highly condensed vanadium species. Higher sodium hydroxide concentration can lead to extrinsic formation of vanadium and does not promote vanadium into the framework structure but rather weakens the crystal structure. Samples prepared with high sodium hydroxide concentration are susceptible to destruction during calcinations. Using the novel silatrane precursor, VS-1 zeolites with high vanadium loading can be prepared via hydrothermal synthesis.

6.2 Introduction

The introduction of various metal ions into the zeolite structure as catalysts has been studied for more than a decade due to its high surface area along with the molecular screening property. Vanadium, a well known catalyst has been added into many kinds of zeolite lattices, including BEA [1-2] MTW [3], MEL [4-5], MFI [6-14], and mesoporous materials like MCM41 [15]. It can be considered that such heteroatoms could be intrinsic to the structure, by replacing some silica atoms in the lattice, or might be extrinsic arising from ionic interaction between the heteroatom and the zeolite surface. Being intrinsic or extrinsic to the lattice has been demonstrated to influence the catalytic properties, c.f. for instance, V-containing silicalite or vanadium oxide supported on silica [16-17].

The different ionic radii of V^{4+} (59 pm) and Si^{4+} (26 pm) atoms makes it more difficult to incorporate vanadium into silica. Thus, defects are produced through lattice distortion upon insertion of the heteroatom.

In general, there are two main methods to prepare vanadium loaded ZSM-5 zeolite. The first is post-synthesis treatment which involves mechanical treatment between H-ZSM5 and V_2O_5 followed by heat treatment [10-11]. This method can be improved to enhance the level of vanadium incorporated into the zeolite structure by either dealumination before treatment or gas phase deposition of vanadium [12]. A second method is hydrothermal synthesis [7-9] having less preparation steps and requiring less special instrumentation for preparation.

Wongkasemjit et al [18-20] have focused on the synthesis of novel metal alkoxides having moisture stable properties, as compared to commercial products. Silatrane and alumatrane are two examples that have been used for the synthesis of silicalite and aluminosilicalite (ZSM5) [21-22]. Because these precursors are moisture stable the hydrolysis rates are therefore slower, resulting in easy handling and control. Using in-house synthetic precursors which differ from those studied by previous scientists, VS-1 was synthesized and the individual factors affecting the properties of the product were studied. The kinetic role of these factors, namely, water content, heating temperature, sodium hydroxide concentration and vanadium concentration loading, were investigated.

6.3 Experimental

Materials

Fumed silica with 99.8% silica content (SiO_2) was supplied from Sigma Chemical. Triethanolamine (TEA, $N[CH_2CH_2OH]_3$) was supplied by Carlo Erba reagenti. Ethylene glycol (EG) used as reaction solvent, was obtained from J.T. Baker. 99% Vanadium (III) chloride (VCl_3) was supplied by ACROS Organics. Sodium hydroxide (NaOH) was purchased from EKA Chemicals. Tetra-propyl ammonium bromide (TPA) was obtained from Fluka Chemical AG. All chemicals were used as received. Acetonitrile (CH_3CN) was obtained from Lab-Scan Co., Ltd. and distilled using standard purification methods prior to use.

Instrumentation

FTIR spectroscopic analysis was conducted using a Bruker Instrument spectrometer (EQUINOX55) with a resolution of 2 cm^{-1} to measure the functional groups of materials. The solid samples were mixed and pelletized with dried KBr. Thermal properties and stability were analyzed using a Perkin Elmer TGA7 analyzer at a scanning rate of 10 K/min under nitrogen atmosphere from 303 to 1023 K. Thermogravimetric/differential thermal analysis was conducted using a Perkin Elmer Pyris Diamond TG/DTA. The crystal morphology was studied using a JEOL 5200-2AE scanning electron microscope. UV-visible measurement was performed using a Shimadzu UV-2550 with the ISR-2200 Integrating sphere attachment and using $BaSO_4$ as reference sample. Crystal structure was characterized using a Rigaku X-Ray Diffractometer at a scanning speed of 5 degree/sec, with CuK line as incident radiation and a filter. The working range was 3-50 theta/2 theta, with 1 degree and 0.3 mm setting of divergence for the scattering and receiving slits, respectively. Reduction of VS-1 was performed using Thermo Finnigan TPDRO 1100 with a flow rate of 20 ml/min of 5.32% Hydrogen in Nitrogen at 10 K/min. The Si/V ratio was determined using X-ray fluorescence spectroscopy (Bruker model SRS 3400), and 99.8% boric acid as binder. Hydrothermal treatment by microwave heating technique was conducted on MSP1000, CME cooperation (Spec 1,000 W and 2450 MHz).

Samples were heated in a Teflon tube, using the inorganic digestion mode, with time-to-temperature programming.

Methodology

Silatrane Synthesis

Silatrane was synthesized and characterized as described elsewhere[21,22] using FTIR, TGA and XRD techniques. FTIR shows the characteristic peaks of product as follows; 3422 cm^{-1} (ν OH), 2986-2861 cm^{-1} (ν CH), 2697 cm^{-1} (ν N→Si), 1459-1445 cm^{-1} (δ CH), 1351 cm^{-1} (ν CN), 1082 cm^{-1} (ν Si-O-C), 1049 cm^{-1} (ν CO), 579 cm^{-1} (ν N→Si). XRD pattern gives the expected pattern as in our previous works [21-22]. Thermal analysis was performed and the percentage of the char yield determined to be 18.36%, close to the theoretical value of 18.4%, corresponding to the structure $Si((OCH_2CH_2)_3N)_2H_2$.

Synthesis of Vanadium Containing Silicate-1 (VS-1)

Vanadium (III) chloride was prepared within a glove box under a dry nitrogen atmosphere before adding SiTEA equivalent to 0.5 g SiO_2 and then adding DI water. The mixture was stirred continuously before adding the template molecule TPA. Sodium hydroxide was added into the mixture while vigorously stirring the mixture. The sample bottles were sealed using double caps covered with extra wrap of aluminum foil, sandwiched by paraffin wrap. To establish the optimum conditions for incorporatation of vanadium into the silicate-1 structure, water content, sodium hydroxide concentration, and temperature were studied. The aging time was fixed at 84 hr at room temperature with continuously stirring and 20 hr of heating under microwave irradiation. The VS-1 as-synthesized products were characterized using XRD and ESR prior to calcination in an electronic furnace set at 550°C with the heating rate of 1°C /min. Calcined products were characterized using UV-VIS and XRD. Before analyzing the samples using ESR at 25°C, calcined samples were washed with 1 N ammonium acetate solution at 75°C for 12 hr and dried under vacuum at 200°C for 2 hr. Washed and un-washed samples were reduced using temperature programmed reduction before characterization by ESR.

6.4 Results and Discussion

Previous works [21-22] show that both aging and heating time play important roles influencing the crystal morphology and size. Smaller crystals with complete conversion of the precursor to zeolite are obtained via longer aging and heating times. Thus, the timing factors were fixed in this work at the optimal condition of 84 and 20 hr aging and heating time, respectively.

Introduction of a foreign atom into the structure of MFI zeolite was studied in previous work where we introduced aluminum into the zeolite structure to obtain strong acid sites within the pore structure [23]. The concentration of NaOH was an important factor for incorporating a large amount of aluminum into the zeolite structure, whereas temperature and water content influenced the morphology and growth rate of zeolite. Thus, the following individual factor were emphasized in this study, namely, water content, temperature of reaction, NaOH concentration in relation to the amount of vanadium loading and the effect on the morphology and localization of vanadium species in the zeolitic structure.

Effect of Water Content

It was shown that water content strongly affects the crystal morphology [21] at the reaction temperature of 150 °C. This reaction temperature is sufficient for complete conversion of precursor to MFI zeolite in a relatively short microwave heating time of 5 hr. The formula used in this study for preparing vanadium containing MFI (VS-1) is 40Si:1V:4TPA-Br:16NaOH, which is comparable to the formula studied in previous works [21-22]. Water content was studied at H_2O/Si ratios of 50, 70 and 100 As shown in figure 6.1, SEM results indicate, as expected, the morphology changes on diluting with water. The nature of the morphological changes differs for VS-1 versus silicalite MFI. Morphological changes of MFI are strongly affected by a change in c-axis, as shown in figure 8c in reference 21. Silicalite tends to form smaller crystals with decreasing water, reflecting a higher rate of nucleation. Evidently, decreasing water content corresponds to a higher concentration of vanadium, sodium hydroxide and template. According to results in ref. 21, higher sodium hydroxide concentration results in more nucleation and

smaller crystals, therefore it appears the larger crystals observed in this work result from decrease of zeolite nucleation due to obstruction by vanadium heteroatoms. The influence on the morphology of adding more vanadium is discussed in the section on the effect of vanadium concentration. This behavior also applies to zeolite synthesis with the same formulation, using other sources of silica, such as tetraethyl orthosilicate (TEOS) and Ludox.

Diffuse reflectance (DR) UV-Visible results of calcined samples are shown in figure 6.2. Low water content increases incorporation of vanadium into the zeolite structure. No absorption band can be detected at the H_2O/Si ratio of 100, but the signal increases with decreasing water content. The UV-Visible spectra of various vanadium compounds are available for comparison with vanadium in VS-1 to show the relationship between absorption spectrum and vanadium species incorporated in the MFI structure [9]. The absorption spectrum of vanadium consists of low-energy charge transfer (LCT) bands associated with electron transfers from O to V. It has been classified into 3 major bands, one in the region between 333-500 nm assigned to V^{5+} ions in octahedral environment, and two in the region 285-333 nm, one assigned to V^{5+} in tetrahedral environment, and one at higher frequency assigned to V^{4+}. Other bands assigned to d-d transitions of VO^{2+} can appear at three different wave numbers, viz. 769 nm for $[b_2(d_{xy})\rightarrow e(d_{xy},d_{yz})]$, around 625 nm for $[b_2(d_{xy})\rightarrow a_1(d_{x2-y2})]$ and higher frequencies for $[b_2(d_{xy})\rightarrow a_1(d_{x2})]$. The presence of extrinsic vanadium in MFI zeolite will be observed at lower energy, indicating presence of V-O-V chains. However, it is difficult to confirm by UV-visible spectra that no extrinsic vanadium is present in the structure due to the weak strength of the d-d transition, generally 10-30 times lower than that of charge transfer transitions. In Figure 6.2, the peak at 285 and the shoulder around 333 indicate the presence of V^{5+} in a tetrahedral environment.

The amount of vanadium incorporated is related to the ability of vanadium to condense together with silica during the sol-gel process in aqueous solution as reported by Livage [24]. The condensation of vanadium is strongly dependent on the amount of water content. This explains our experiment at the H_2O/Si ratio of 100. The condition is too dilute for vanadium species to condense with silica. Thus, the condensation can be enhanced by decreasing water content.

Effect of Temperature

It is well known that temperature is an important factor for both nucleation and especially growth rate in MFI zeolite [23]. Therefore, MFI synthesis using silatrane at different temperatures was studied [21]. Silicalite from silatrane has previously been studied via synthesis by microwave heating in the temperature range 120° to 180°C. Although VS-1 can be synthesized at temperatures as high as 210°C, as in the study of Miyamoto et al. [8], problems arose due to Hoffman degradation of the template molecule, resulting in uncontrollable pressure build-up. However, this can be prevented by performing synthesis under an inert atmosphere, such as nitrogen gas. In our experiment, the same formulation as used above was purged with nitrogen gas before heating at 180°C for 20 hr.

It is also known that increased temperature obviously affects the growth rate and the product morphology [21, 23], and also enhances the condensation of transition metal [24], as demonstrated, respectively, in figure 6.3 by SEM and figure 6.4 by UV-visible spectroscopy. As observed at lower temperature (figure 6.1), crystal size increases with decreasing water content, however, figure 6.3 shows that higher temperature results in larger crystals of VS-1 due to growth rate enhancement. Comparing figures 6.1 and 6.4, we see a dramatic increase of absorbance at both 285 nm and 333 nm, assigned to V^{5+} in a tetrahedral environment as discussed in the previous section.

Figures 6.2 and 6.4 are strong evidence that increase in temperature increases the condensation of vanadium into zeolite; however, at H_2O/Si ratio equal to 100, the spectrum shows a shoulder as the temperature increases. ESR spectra of VS-1, as-synthesized at high reaction temperature for each water content are illustrated in figure 6.5 and show eight nearly, equally spaced lines arising from hyperfine splitting of the d electrons with I = 7/2 spin for all water contents. The anisotropic hyperfine electron resonance signal at room temperature indicates that the vanadium species are relatively immobile. Evidently, vanadium present within the MFI structure, as isolated vanadyl species in square pyramidal or distorted octahedral coordination, is observed via ESR at room temperature. However, the

spectrum at the lowest H_2O/Si ratio appears to have a small amount of a superimposed singlet that signal the onset of extrinsic vanadium formation.

Following the above results the effects of sodium hydroxide concentration and vanadium loading were studied by setting the reaction temperature at 180°C and the water content at 50 and 70 H_2O/Si.

Effect of Sodium Hydroxide Concentration

SEM results are shown in figure 6.6, for specimens synthesized using a mole ratio of Si:V:TPA-Br equal to 40:1:0.4, and sodium hydroxide concentration varied at NaOH ratios of 12, 16 and 20, together with H_2O/Si at two mole ratios of 70 and 50. Recalling that the effect of decreasing water content is analogous to an increase in sodium hydroxide, we need to reconcile the facts that, at fixed H_2O/Si, the crystal size increases with decreasing sodium hydroxide concentration (figure 6.6a-6.6c), and yet, with lower water content at fixed ratios of sodium hydroxide (figure 6.6d-6.6f and also figures 6.1 and 6.3), larger crystal sizes are obtained. Note, however, at too high a sodium hydroxide concentration, the crystals become fragile due to a greater possibility to redissolve back into the supersaturated solution during heating [23] which agrees with observations in ref. 21.

From previous work [22] which considered the individual contributions of sodium cation and hydroxide anion, we find that sodium ion concentration influences the nucleation process in the initial stages of the reaction by stabilizing the oligomeric species of polysilicate anion prior to formation of the primary particle. Thus, increasing sodium ion tends to promote more nucleation, resulting in smaller crystals. However, too much sodium ion has the harmful effect of lowering conversion due to interference in the reaction between template molecule and polysilicate anion. In the present study, from both XRD and SEM results, such a phenomenon was not observed since increase in sodium cations was accompanied by increase in hydroxide anions. Generally, smaller crystal sizes are obtained by increasing hydroxide concentration, resulting in decreasing yield [25]. The effect of these two factors is that the crystal size becomes rather small with increase of NaOH concentration at fixed H_2O/Si, as seen in figure 6. With regard to the larger size of VS-1 at lower water content, this results from obstruction of zeolite nucleation by

vanadium heteroatoms, possibly due to the presence of the oxovanadium (IV) compound $[VO(H_2O)_5]^{2+}$ or the aqua ion of $[V(H_2O)_6]^{3+}$ in vanadium containing MFI during nucleation [26].

UV-visible results on these samples are shown in figure 6.7 labelled according to figure 6.6. Ii is clear that the amount of vanadium increases with decreasing sodium hydroxide for both water contents, related to the enhanced condensation ability of vanadium, which also depends, however, on the mixture pH, as reported by Livage and coworkers [24,27] in studies of the sol-gel chemistry of metal oxide by Livage et al [27] and the sol-gel synthesis of heterogeneous catalysts [24]. Livage et al [24] develoed a charge-pH diagram delineating three domains in which aqua (H_2O), hydroxo (OH^-) and oxo (O^{2-}) ligands are formed. Fundamentally, condensation occurs in the region having the hydroxo ligand. The occurrence of this ligand depends on the oxidation stage and pH range. Defining an appropriate pH range, which corresponds to the oxidation stage of the transition metal, is the key to condensation. This pH sensitivity correlates to our observation that too high a sodium concentration provides less condensation, as observed by less signal intensity in the UV-visible spectrum. However, too low a sodium hydroxide concentration at the ratio of NaOH/V = 8 causes incomplete conversion of precursor to zeolite as indicated by the presence of amorphous material in the product (SEM and XRD results are not shown). Thus, the appropriate ratio of NaOH/V in this experiment is around 12.

The ESR spectra of the as-synthesized samples in figure 6.8a are essentially the same as those in Figure 6.5b, showing a well defined hyperfine splitting. ESR parameters of vanadium-containing MFI are listed in table 6.1. The normalized value of double integrated spectra gave the same trend as the UV-visible results i.e. that the amount of vanadium in the VS-1 increased with decreasing sodium hydroxide concentration. Other parameters, namely, the g factor and hyperfine coupling constant for both parallel and perpendicular directions, show no significant differences between as synthesized samples shown in Figure 6.5b and 6.8a, though different sodium hydroxide concentration were used, indicating no difference in environment around the vanadium in the VS-1 zeolite. However, the g factors show a small difference after treatment with ammonium acetate, which is discussed in detail

in the next section. ESR spectra reversible between as-synthesized and reduced/calcined samples (Figures 6.8a and 6.8c) demonstrate redox behavior of the vanadium in the sample which could be used in the reaction of oxidative dehydrogenation.

The effect of sodium hydroxide concentration on the amount of vanadium incorporated into the MFI structure was investigated using XRF as summarized in the Table 6.2. The results are consistent with the results obtained by UV-Vis and ESR that the amount of vanadium is increases with decrease of sodium hydroxide concentration for both untreated samples and those treated with 1N ammonia acetate. However, the amount of the vanadium in treated samples synthesized at high sodium hydroxide concentration shows a greater decrease than those made using lower sodium hydroxide concentration. This result shows that extrinsic vanadium species are more prevalent in the system using high sodium hydroxide concentration. Increase in sodium hydroxide concentration is equivalent to a decrease in water content, see figure 6.5a. The hyperfme splitting ESR spectrum is super-imposed on a singlet, which is in fact a sign of extrinsic vanadium formation.

All of the as-synthesized VS-1 was characterized using XRD, as shown in figure 6.9. It was found that all samples show peaks characteristic of MFI topology. However, after calcination even at a very slow rate (0.5 degreeC/min) samples formulated with a high concentration of sodium hydroxide and vanadium show several extra peaks with two major ones at around 21.84 and 36.04 2theta/theta, indicating a decay of MFI structure. The degree of decay depends on the concentration of sodium hydroxide, vanadium, and water content. The formulation having Si/V and H_2O/Si equal to 25 and 50, respectively, and high sodium hydroxide concentration (NaOH/Si = 0.3-0.5), gives severe decay of zeolite after calcination. Lowering the vanadium loading amount (Si/V=40) and sodium hydroxide concentration (analogous to higher water content, H_2O/Si=70) decreases the susceptibility to structure decay after calcination (figure 6.9a), as compared to a lower water content (H_20/Si=50) shown in figure 6.9b.

From previous study [21] high sodium hydroxide concentration causes fracture and fuse formation in the silicalite system. In fact, both high concentration of the sodium hydroxide and high temprature redissolve the growing zeolite into the

supersaturated solution during synthesis, possibly leading to higher defect levels in the structure of the zeolite crystal. In this case, high vanadium loading resulting in condensation of vanadium into the zeolite structure can be considered as creating defects, producing higher stress in the framework structure due to the large atomic size of vanadium as compared to that of silicon.

It is obvious that higher sodium hydroxide concentration not only leads to the extrinsic formation of vanadium, but also will not promote insertion of vanadium into the framework structure. Rather it weakens the crystal structure, making the crystals susceptible to be destroyed during calcination.

The novel silatrane precursor shows unique and distinctive properties, as described previously [21-22]. One extraordinary property obtained using silatrane is that it produces uniform crystals of smallest size, when compared to other silica sources such as tetraethyl orthosilicate, and fumed silica. Moreover, it shows higher performance for preparation of high aluminum loading in ZSM-5 [22]. The present work shows that silatrane as precursor provides remarkably higher potential to produce high vanadium loading, as listed in table 6.2.is the loading can be almost as high as 1 vanadium atom per 3 unit cell of MFI, a level that has been previously difficult to obtain via the hydrothermal synthesis.

Effect of Vanadium Concentration

SEM results of the effect of increasing the sodium hydroxide concentration on samples with increased vanadium loading (Si/V=25) are shown in figure 6.10. The results can be compared with those in figures 6.6a-c at decreased vanadium loading (Si/V=40). The morphology of the VS-1 at higher loading shows larger crystal sizes (figure 6.10), in agreement with previous discussion that increasing vanadium results in larger crystal sizes due to less nucleation. Moreover, as noted earlier for lower vanadium loading, the crystal size increases with decrease in the hydroxide concentration also at high V loading.

The quantity of vanadium incorporated into the MFI framework structure was investigated by the XRF technique, and the results are given in table 6.2. The amount of vanadium of untreat ammonium acetate at low vanadium loading and ammonium acetate treated samples at high vanadium loading, does not show a

significant difference. Moreover, the ESR spectrum shown in figure 6.11c (with Si/V ratio of 25) shows a similar amplitude to that of the treated sample at lower vanadium loading in figure 6.8c (with Si/V ratio of 40). The V(IV) intensity of the ESR spectra is lower than it should be, according to the XRF result. The reason may arisee from the fact that tetrahedrallly coordinated vanadium can not be detected by ESR at room temperature due to its short relaxation time. More than half the vanadium species after reduction and treatment with ammonium acetate could be present in the form of tetrahedrally coordinated species [28]. Likewise, the hyperfine coupling constant and g factor show no change at room temperature with change in the vanadium concentration.

With decreasing water content, the hyperfine coupling is not changed while the g factor seems to decrease, see figure 6.5a. However, this result is ambiguous, because broadening of the spectra causes the g factor to be less well resolved. However, both hyperfine coupling constant and g factor are changed after treatment with ammonium acetate at all vanadium loadings. With regard to the g factor and hyperfine coupling constant, it is known that the distance between vanadium and oxygen in VO^{2+} group is directly related to the $\Delta g_{\parallel}/\Delta g_{\perp}$ ratio and the hyperfine component $A_{\parallel}$ [29-30]. Increase of the $\Delta g_{\parallel}/\Delta g_{\perp}$ ratio or the hyperfine coupling $A_{\parallel}$ is a sensitive indicator of tetragonal distortion via a decrease in the V=O bond, or an increase in the distance between the four oxygen ligands in the basal plane. The ratio $\Delta g_{\parallel}/\Delta g_{\perp}$ can be calculated according to the following equation;

$$\frac{\Delta g_{\parallel}}{\Delta g_{\perp}} = \frac{(g_{\parallel} - g_e)}{(g_{\perp} - g_e)}$$

In our case, comparing figures 6.8b and 6.8c, after extraction of the extrinsic vanadium by ammonium acetate, it was found that the $\Delta g_{\parallel}/\Delta g_{\perp}$ ratio and hyperfine constant $A_{\parallel}$ increase from 2.8 to 4.9 and 118.3 to 124.3, respectively. Higher vanadium loading in figure 6.11 also gives higher values of the $\Delta g_{\parallel}/\Delta g_{\perp}$ ratio and $A_{\parallel}$. From these data, it can be seen that intrinsic vanadium causes more lattice distortion. After leaching out the extrinsic vanadium, it is likely that some vanadium sites are modified such that the terminal bridges with silica atoms are broken to form

hydroxyl group terminals, resulting in an increase of $\Delta g_{\parallel}/\Delta g_{\perp}$ or $A_{\parallel}$, based on previous reports that an increase of $\Delta g_{\parallel}/\Delta g_{\perp}$ occurs when vanadium interacts with water molecule, forming terminal hydroxyl groups [15].

6.5 Conclusions

VS-1 zeolite was synthesized using silatrane as precursor and the factors studied that influence the properties of the product. Lower water content with higher reaction temperature is the preferable condition for VS-1 synthesis due to higher promotion of vanadium condensation into the zeolite structure. The amount of sodium and vanadium loading strongly influences the amount of intrinsic vanadium species within the VS-1 zeolite. Lower sodium hydroxide concentration gives higher vanadium in the structure, with less leached out, when compared to VS-1 formed using a high sodium hydroxide concentration. Therefore high sodium hydroxide increases extrinsic vanadium formation and does not promote incorporation of vanadium into the framework structure. Samples prepared with high sodium hydroxide concentration are susceptible to destruction during calcination. ESR spectroscopy at room temperature shows that the vanadium species in all samples are immobilized and well dispersed in the MFI structure. Thus, the silatrane precursor provides good potential for preparing VS-1 zeolite with high vanadium loading via the hydrothermal synthesis method.

6.6 Acknowledgements

This research work was supported by the Postgraduate Education and Research Program in Petroleum and Petrochemical Technology (ADB) Fund, Ratchadapisake Sompote Fund, Chulalongkorn University and the Thailand Research Fund (TRF).

6.7 References

[1] S. Dzwigaj, M. Matsuoka, R. Franck, M. Anpo, M. Che, J. Phys. Chem. B 102 (1998) 6309.

[2] S. Dzwigai, M. Matsuoka, M. Anpo, M. Che, J. Phys. Chem. B 104 (2000) 6012

[3] I.L. Moudrakovski, A. Sayari, C. I. Ratcliffe, J. A. Ripmeester, K.F. Preston, J. Phys. Chem. 98 (1994) 10895

[4] T. Sen, V. Ramaswamy, S. Ganapathy, P.R. Rajamohanan, S. Sivasanker, J. Phys. Chem. 100 (1996) 3809

[5] P.R. H.P. Rao, A.A. Belhekar, S.G. Hegde, A.V. Ramaswamy, P. Ratnasamy, J. Catal. 141 (1993) 595

[6] M.S. Rigutto, H.V. Bekkum, Appl. Catal. 68 (1991) L1

[7] P. Fejes, I. Marsi, I. Kiricsi, J. Halasz, I. Hannus, A. Rockenbauer, Gy. Tasi, L. Korecz, Gy. Schobel, in: P.A. Jacobs, N.I. Jaeger, L. Kubelkova and B. Wichterlova (Eds.), Zeolite Chemistry and Catalysis, Studies in Surface Science an Catalyst, Vol. 69, Elsevier, Amsterdam, 1991, p.173

[8] A. Miyamoto, D. Medhanavyn, T. Inui, Appl. Catal. 28 (1986) 89

[9] G. Centi, S. Perathoner, F. Trifiro, A. Aboukais, C.F. Aissi, M. Guelton, J. Phys. Chem. 96 (1992) 2617

[10] M. Petras, B. Wichterlova, J. Phys. Chem. 96 (1992) 1805

[11] S.G. Zhang, S. Higashimoto, H. Yamashita, M. Anpo, J. Phys. Chem. B 102 (1998) 5590

[12] B.I. Whittington, J.R. Anderson, J. Phys. Chem. 95 (1991) 3306

[13] A. Tavolaro, Desalination 147 (2002) 333

[14] A. Julbe, D. Farrusseng, J.C. Jalibert, C. Mirodatos, C. Guizard, Catal. Today 56 (2000) 199

[15] H. Berndt, A. Martin, A. Bruckner, E. Schreier, D. Muller, H. Kosslick, G.U. wolf, B. Lucke, J. Catal. 191 (2000) 384

[16] A.V. Kucherov, A.V. Ivanov, T.N. Kucherova, V.D. Nissenbaum, L.M. Kustov, Catal. Today 81 (2003) 297

[17] M. Anpo, S. Higashimoto, M. Matsuoka, N. Zhanpeisov, Y. Shioya, S. Dzwigaj, M. Che, Catal. Today 78 (2003) 211.

[18] B. Ksapabutr, Erdogan Gulari, and Sujitra Wongkasemjit, *Materials Chemistry and Physics*, 83/1 (2004) 34-42

[19] N. Phonthammachai, T. Chairassameewong, E. Gulari, A.M. Jamieson, and S. Wongkasemjit, *J.Metals, Minerals and Materials, Chulalongkorn University*, 12(1) (2002) 23-28.

[20] Yukoltorn Opornsawad, Bussarin Ksapabutr, Sujitra Wongkasemjit* and Richard Laine, *Eur. Polym. J.*, 37/9 (2001) 1877-1885.

[21] P. Phiriyawirut, R. Magaraphan, A.M. Jamieson, S. Wongkasemjit, Mater. Sci. Eng. A 361 (2003) 147

[22] P. Phiriyawirut, R. Magaraphan, A.M. Jamieson, S. Wongkasemjit, Micropor. Mesopor. Mater. 64 (2003) 83

[23] R.W. Thompson, Molecular Sieves 1 (1998) 1

[24] J. Livage, Catal. Today 41 (1998) 3

[25] A. Pfenninger, Molecular Sieves 2 (1999) 163

[26] Cotton A.F., Wilkinson G., Advanced Inorganic Chemistry, 4^{th} edition, John Wiley & Son, New York, 1980, p.714.

[27] J. Livage, M. Henry, C. Sanchez, Prog. Solid St. Chem. 18 (1988) 259

[28] N. Venkatathri, Appl. Catal. A 242 (2003) 393

[29] P.S. Singh, R. Bandyopadhyay, B.S. Rao, J. Mole. Catal A 104 (1995) 103

[30] V.K. Sharma, A. Wokaun, A. Baiker, J. Phys. Chem. 90 (1986) 2715.

CAPTIONS OF TABLE AND FIGURES

Table 6.1

NaOH/ V ratio	Normalized double integrated spectrum	$g_{\|}$	$g_{\perp}$	$A_{\|}$ (G)	$A_{\perp}$ (G)
12	4.30 E+5	1.9165	1.9745	209.3	74.4
16	3.33 E+5	1.9175	1.9751	209.4	74.1
20	2.70 E+5	1.9169	1.9722	209.0	74.2

Table 6.2

Si/V loading	NaOH/Si loading	Si/V	
		Calcined sample	After treated by 1N NH_4OAc
40	0.3	281	477
40	0.5	384	880
25	0.3	122	284

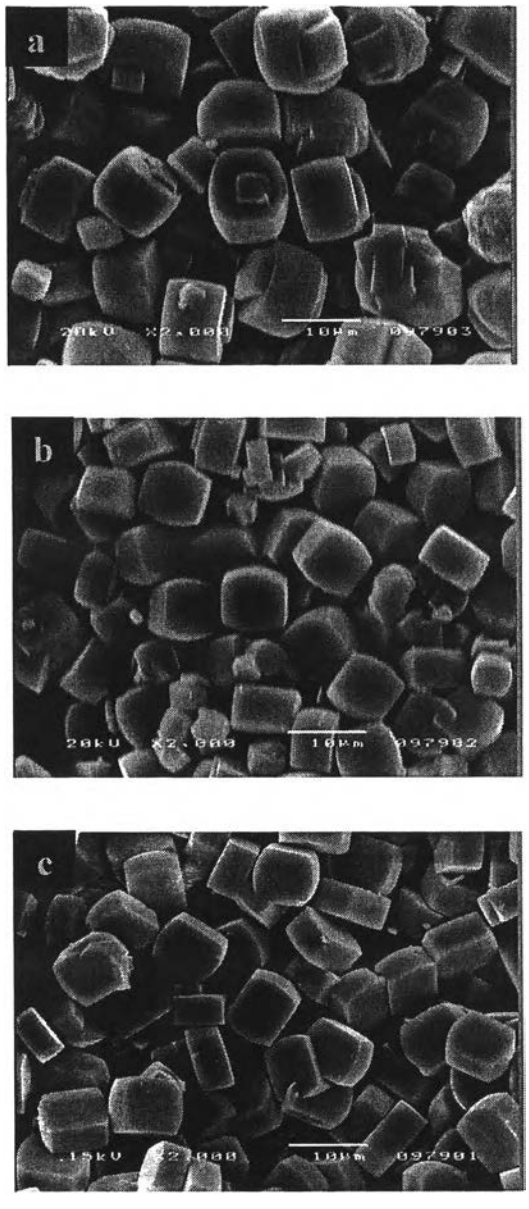

Figure 6.1

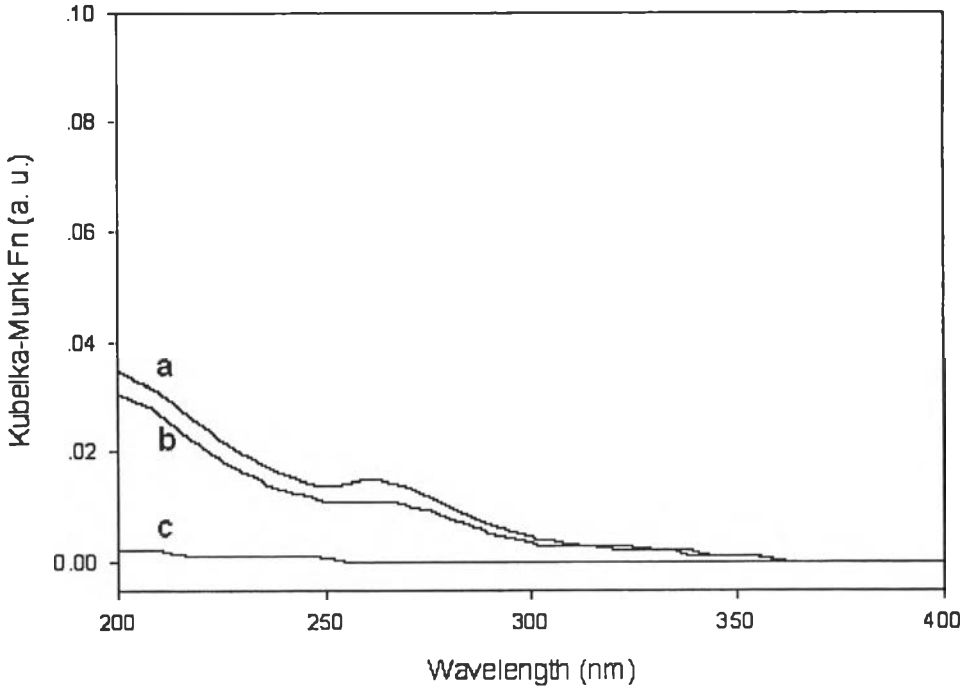
.10
.08
.06
.04
.02
0.00
Kubelka-Munk Fn (a. u.)
a
b
c
200
250
300
350
400
Wavelength (nm)

Figure 6.2

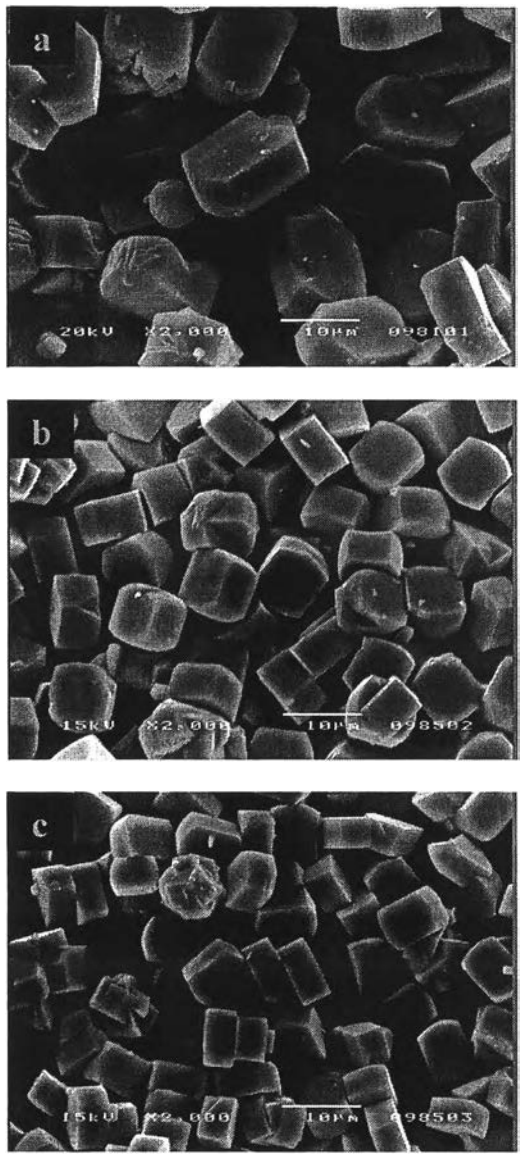
a
20kV X2,000 10μm 098101
b
15kV X2,000 10μm 098502
c
15kV X2,000 10μm 098503

Figure 6.3

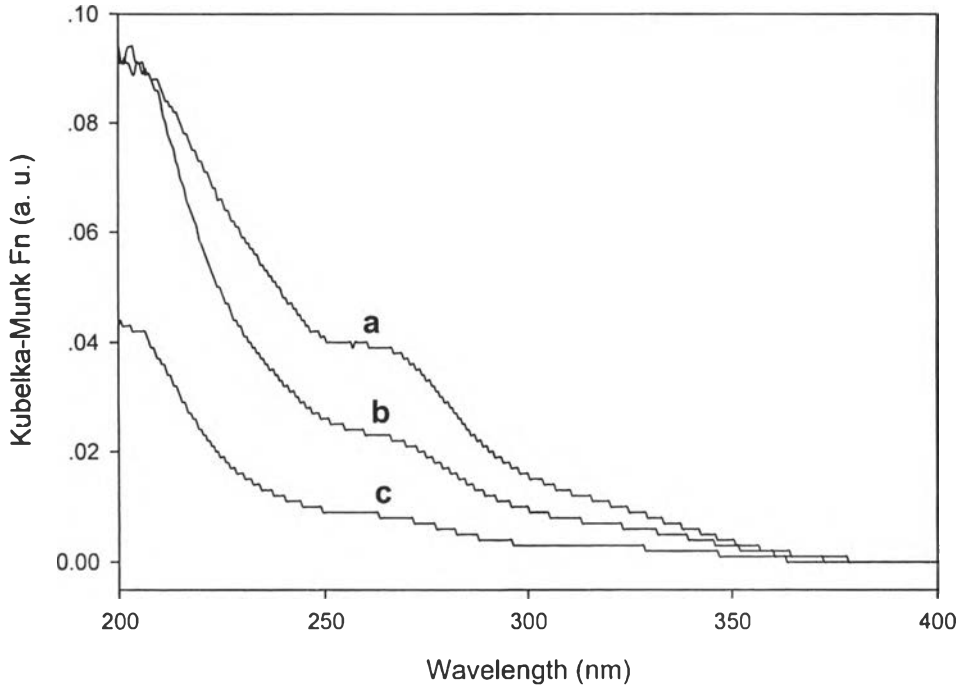
.10
.08
.06
.04
.02
0.00
Kubelka-Munk Fn (a. u.)
a
b
c
200
250
300
350
400
Wavelength (nm)

Figure 6.4

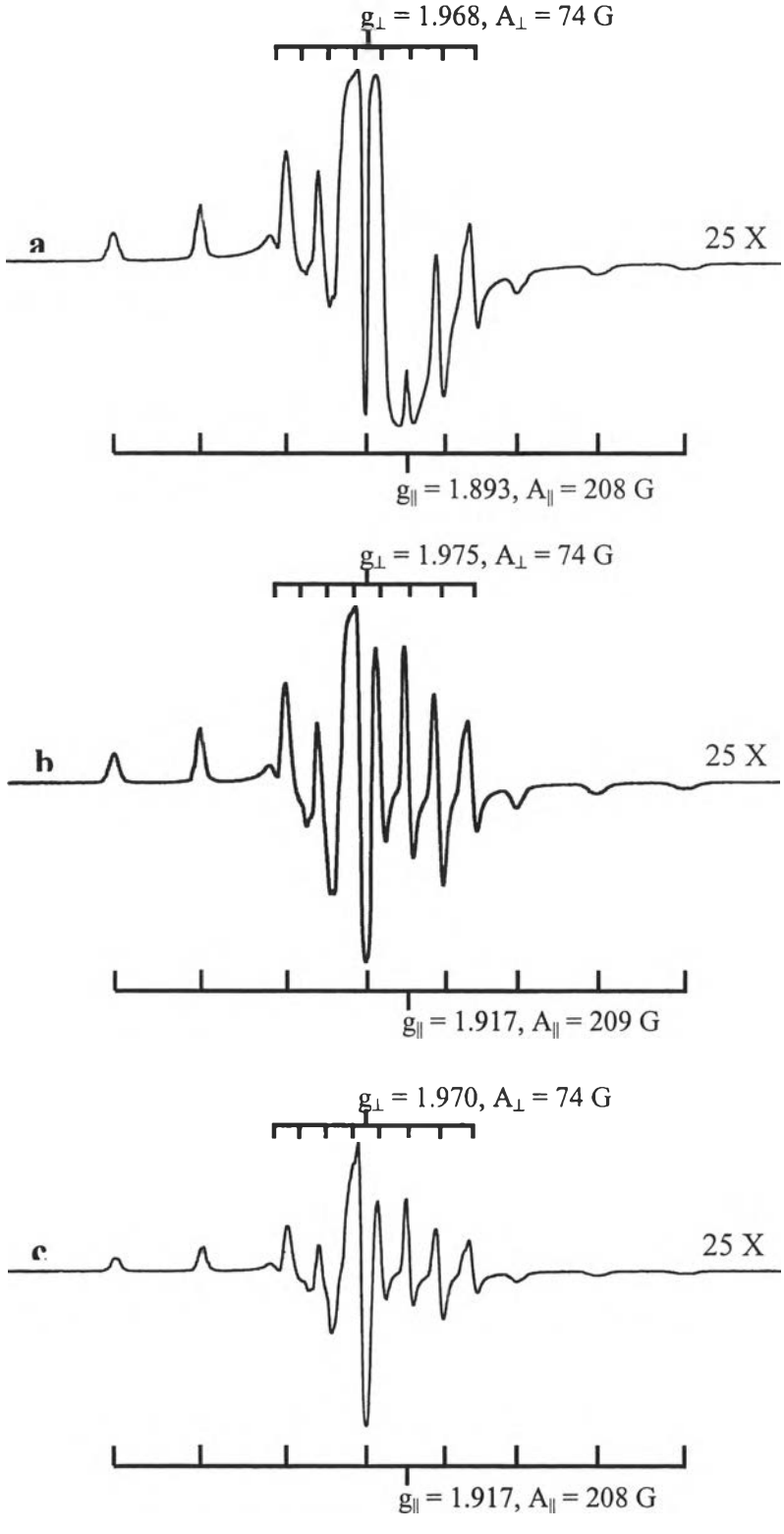
$g_\perp$ = 1.968, $A_\perp$ = 74 G
a
25 X
$g_\parallel$ = 1.893, $A_\parallel$ = 208 G
$g_\perp$ = 1.975, $A_\perp$ = 74 G
b
25 X
$g_\parallel$ = 1.917, $A_\parallel$ = 209 G
$g_\perp$ = 1.970, $A_\perp$ = 74 G
c
25 X
$g_\parallel$ = 1.917, $A_\parallel$ = 208 G

Figure 6.5

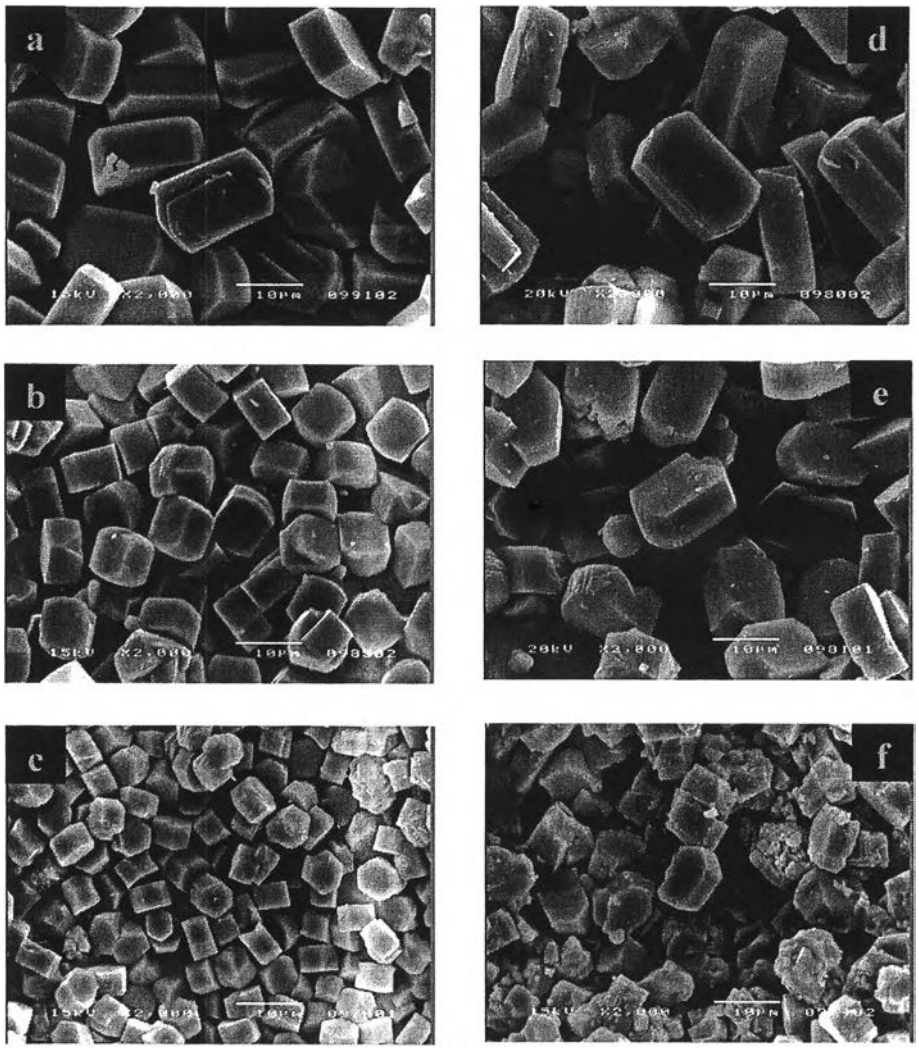

Figure 6.6

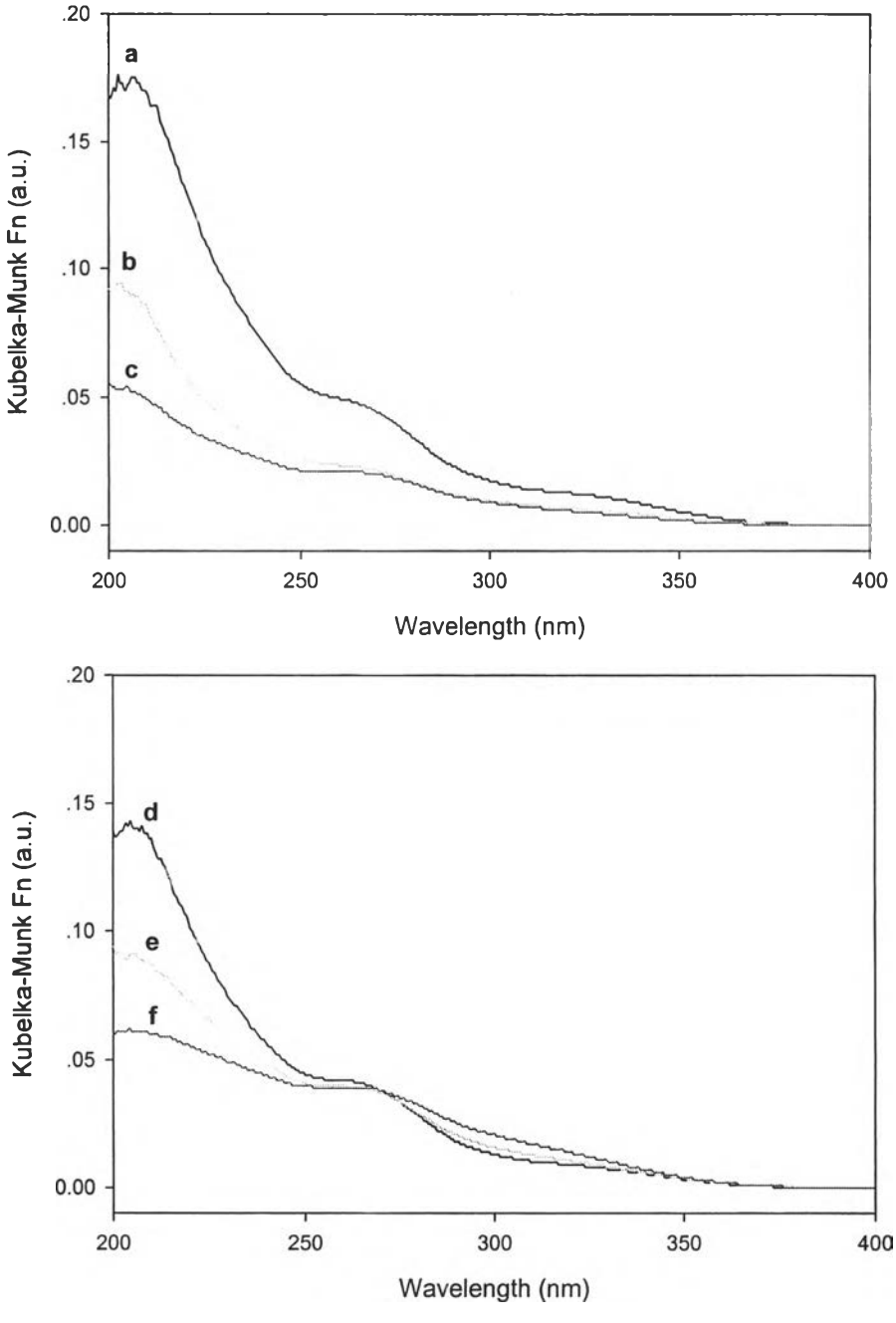
.20
.15
.10
.05
0.00
Kubelka-Munk Fn (a.u.)
a
b
c
200
250
300
350
400
Wavelength (nm)
.20
.15
.10
.05
0.00
Kubelka-Munk Fn (a.u.)
d
e
f
200
250
300
350
400
Wavelength (nm)

Figure 6.7

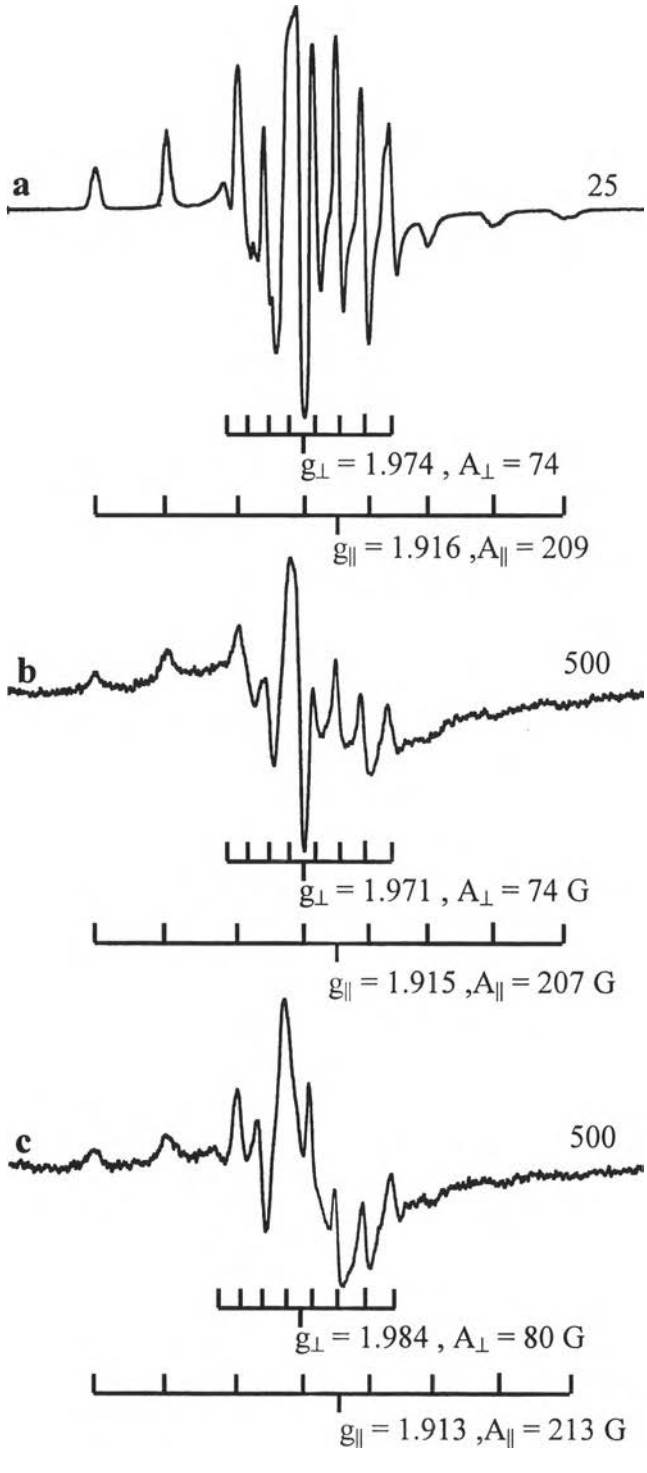
a
25
$g_\perp$ = 1.974 , $A_\perp$ = 74
$g_\parallel$ = 1.916 ,$A_\parallel$ = 209
b
500
$g_\perp$ = 1.971 , $A_\perp$ = 74 G
$g_\parallel$ = 1.915 ,$A_\parallel$ = 207 G
c
500
$g_\perp$ = 1.984 , $A_\perp$ = 80 G
$g_\parallel$ = 1.913 ,$A_\parallel$ = 213 G

Figure 6.8

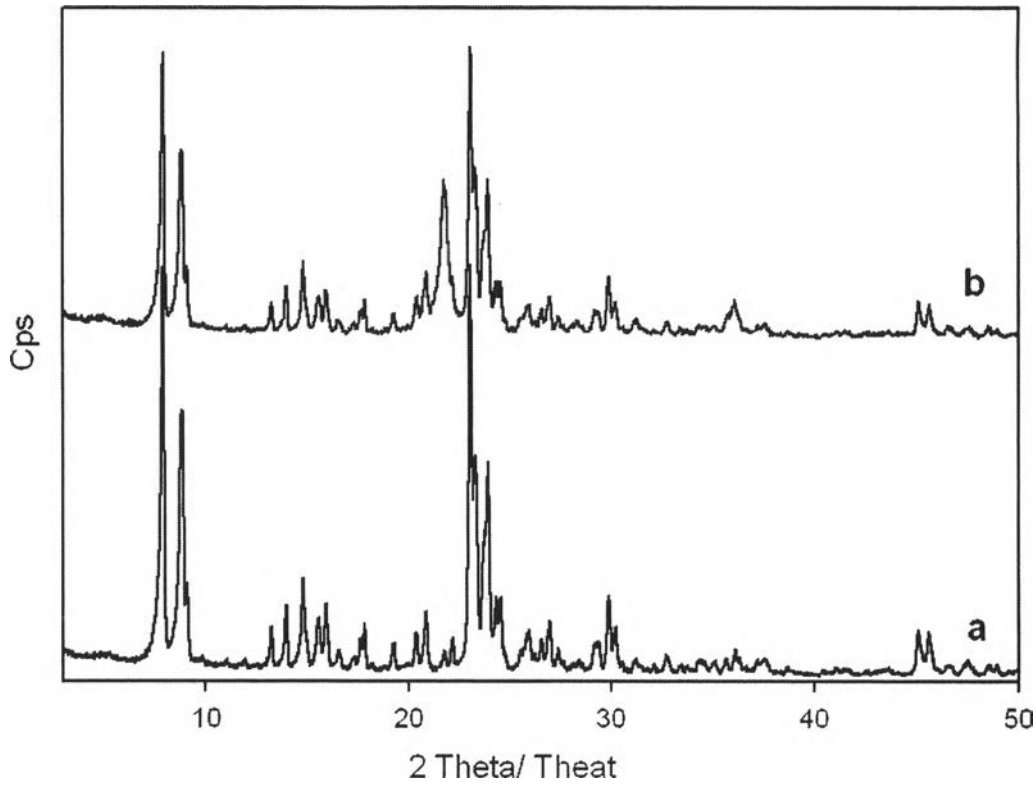

Figure 6.9

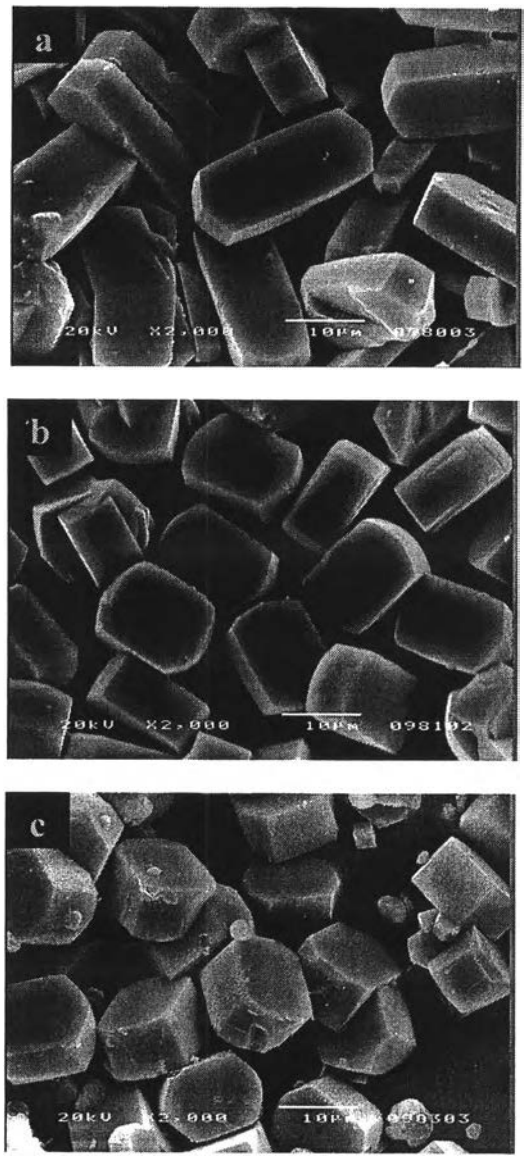
a
20kV X2,000 10µm 078003
b
20kV X2,000 10µm 098102
c
20kV X2,000 10µm

Figure 6.10

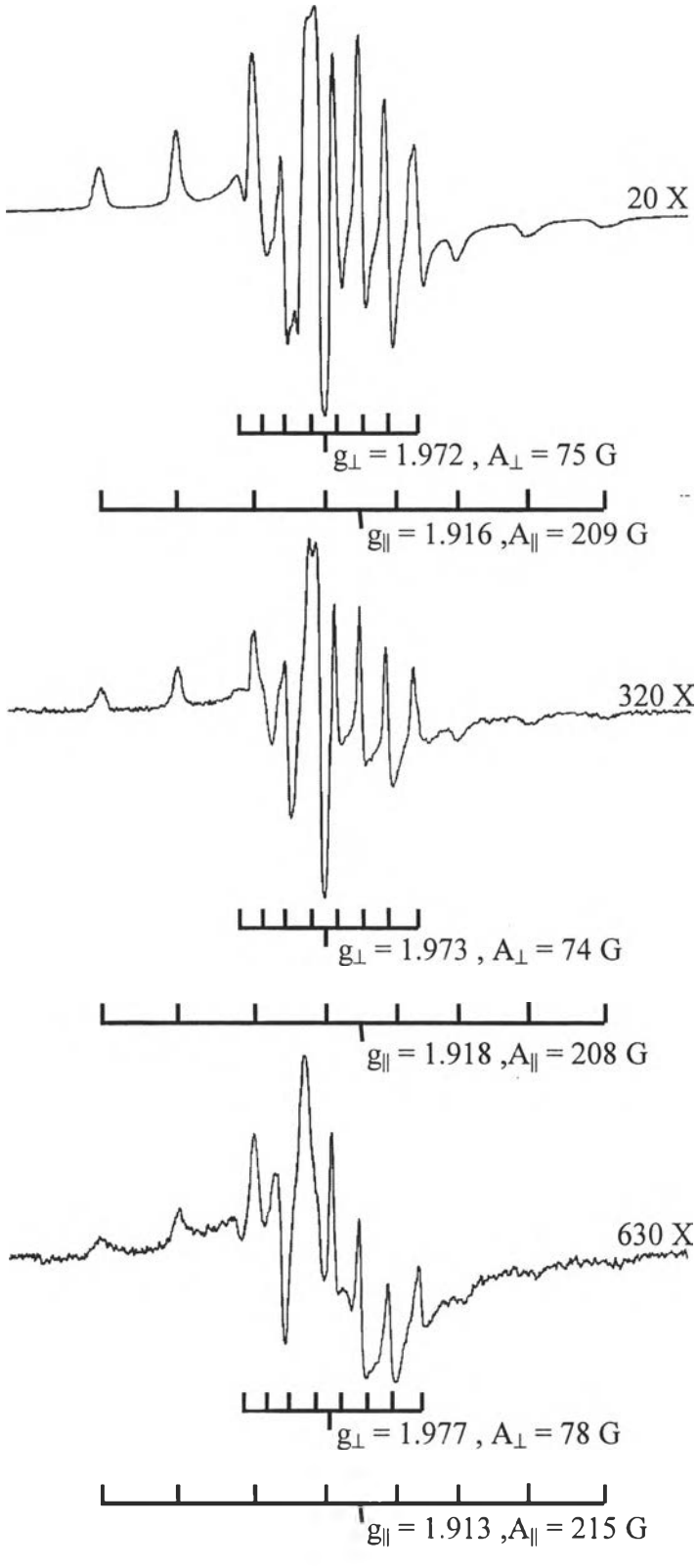
20 X
$g_\perp$ = 1.972 , $A_\perp$ = 75 G
$g_\parallel$ = 1.916 ,$A_\parallel$ = 209 G
320 X
$g_\perp$ = 1.973 , $A_\perp$ = 74 G
$g_\parallel$ = 1.918 ,$A_\parallel$ = 208 G
630 X
$g_\perp$ = 1.977 , $A_\perp$ = 78 G
$g_\parallel$ = 1.913 ,$A_\parallel$ = 215 G

Figure 6.11